Dalton Transactions

Cite this: DOI: 10.1039/c2dt30455d

www.rsc.org/dalton

PAPER

Heterolytic addition of E–H bonds across Pt–P bonds in Pt *N*-heterocyclic phosphenium/phosphido complexes†

Baofei Pan, Mark W. Bezpalko, Bruce M. Foxman and Christine M. Thomas*

Received 24th February 2012, Accepted 16th April 2012
DOI: 10.1039/c2dt30455d

The reactivity of E–H bonds (E = S, O, Cl) with Pt(II) complexes ligated by an *N*-heterocyclic phosphido-containing diphosphine ligand have been investigated. Addition of PhSH to [(PPP)Pt(PPh$_3$)][PF$_6$] (**1**) results in clean formation of [(PP(H)P)Pt(SPh)][PF$_6$] (**3**), in which the substrate has added across the Pt–P^{NHP} bond. Similar reactivity occurs when **1** is treated with ROH (R = Ph, Me), but in this case the O–H bond adds across the Pt–P bond in the opposite direction producing [(PP(OR)P)Pt(H)(PPh$_3$)][PF$_6$] (R = Ph (**4**), Me (**5**)). HCl addition to **1** cleanly generates [(PP(H)P)PtCl][PF$_6$] (**6**^{PF6}). The neutral Pt–NHP complex (PPP)PtCl (**2**) exhibits similar reactivity; however, in the presence of the nucleophilic Cl$^-$ anion, the (PP(OR)P)Pt(H)Cl species presumably generated *via* addition of ROH (R = Me, Et) undergoes an Arbuzov-like dealkylation reaction to exclusively form the *N*-heterocyclic phosphinito species (PP(O)P)Pt(H) (**7**).

Introduction

The facile activation of σ bonds presents an ongoing challenge to synthetic chemists in terms of both organic synthesis and renewable energy applications. In response to this challenge, a recent promising strategy has emerged based on the concept of Frustrated Lewis Pairs (FLPs), allowing combinations of strong Lewis acids and Lewis bases with the proper steric constraints to perform unusual σ bond activation processes in the absence of transition metals.[1–4] An alternative approach that does make use of transition metals is the linkage of a transition metal fragment to a strong Lewis acid *via* a ligand scaffold to generate M → E platforms in which an electron-rich transition metal donates electron density to a tethered main group Lewis acidic atom such as B[5–14] or Sb.[15–19] Rather than steric "frustration", the constraint in these systems is electronic in nature, since even the most electron-rich transition metal fragments still maintain an electropositive character. While the interactions in metal–Lewis acid complexes are still being explored at the very fundamental level, there have been several reports of reactivity in which substrates add oxidatively either across the M → E bond or directly to the Lewis acidic main group functionality.[9,11,13,17,19] In a sense, the early/late heterobimetallic compounds recently reported in our own group display similar electronic structure and reactivity.[20]

Inspired by the success of both FLPs and metal–Lewis acid complexes, we chose to investigate a different type of Lewis acid functionality, *N*-heterocyclic phosphenium cations (NHP$^+$s). These cationic P-containing analogues of *N*-heterocyclic carbenes are strongly Lewis acidic owing to their cationic charge and the empty non-bonding orbital remaining on phosphorus.[21–23] Moreover, their electronic properties render them excellent π-acceptors yet poor σ-donors, in stark contrast to NHCs.[24–26] Notably, attempts in our lab to utilize NHP$^+$s as the Lewis acidic half of a FLP system were unsuccessful, suggesting that they are weaker acids than B(C$_6$F$_5$)$_3$.[27] Nonetheless, we did choose to incorporate an NHP unit into the central position of a chelating diphosphine pincer ligand to investigate M → P interactions and reactivity of metal–NHP complexes.[28] Interestingly, we found that coordination of the NHP–diphosphine ligand to electron rich fragments such as Co^{-1}(CO)$_2$, Pd^0(PPh$_3$), or Pt^0(PPh$_3$) resulted in complexes with an unusual pyramidal geometry about the central NHP unit.[29,30] Structural and computational studies revealed that this geometry was indicative of a stereochemically active lone pair on phosphorus, and thus an NHP$^-$ phosphido description. Further experimental and theoretical investigations suggest that oxidation/reduction and ligand coordination/dissociation can lead to interconversion of NHP$^+$ and NHP$^-$ configurations, similar to the archetypal non-innocent nitrosyl ligand NO$^+$/NO$^-$ (Scheme 1).[30]

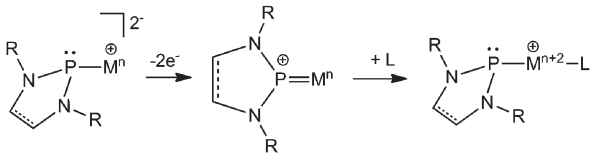

Scheme 1 Interconversion of NHP$^+$ and NHP$^-$ coordination modes.

Brandeis University, Department of Chemistry, 415 South Street MS015, Waltham, MA, USA. E-mail: thomasc@brandeis.edu; Fax: +1 (781) 736-2516; Tel: +1 (781)736-2576

† Electronic supplementary information (ESI) available: Additional computational and spectral details and complete crystallographic data in CIF format for **4**, **6**^{PF6}, and **7**. CCDC 869435–869437. For ESI and crystallographic data in CIF or other electronic format see DOI: 10.1039/c2dt30455d

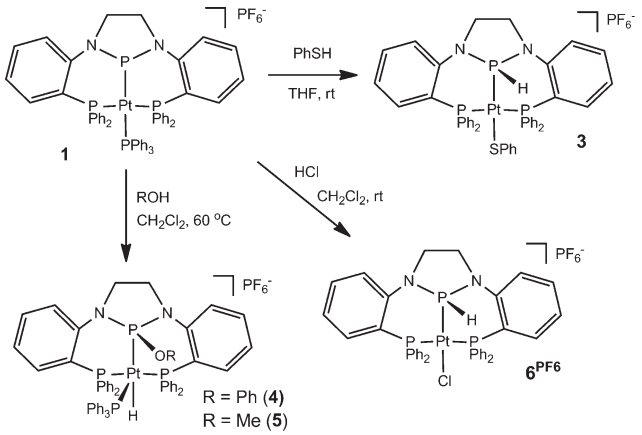

Scheme 2 Addition of E–H bonds to **1**.

We now turn our attention to the addition of substrates to metal–NHP complexes, with specific attention to addition of substrates across the metal–P^{NHP} bond. Several examples of 1,2-addition of substrates across the Pd–amide bond in (PNP)Pd complexes were recently reported by Ozerov and coworkers.[31] To the best of our knowledge, there are no reported examples of E–H (E = S, O) bond activation by FLPs, however, Stephan and coworkers did show that disulfides RSSR are heterolytically cleaved by mixture of $B(C_6F_5)_3$ and P^tBu_3 to give $[^tBu_3PSR]^+$-$[(C_6F_5)_3BSR]^-$.[32] There are also no reported examples of E–H addition to metal–NHP complexes. While the ability of our Pt–NHP complexes to interconvert between NHP^- phosphide and NHP^+ phosphenium configurations leads to some ambiguity in predicting reaction pathways, several reported examples of the addition of ROH and RSH across M–P bonds in M=PR_2 phosphido complexes provide good examples for comparative purposes.[33–37]

Results and discussion

Heterolytic cleavage of E–H bonds by $[(PPP)Pt(PPh_3)]^+$ (1)

Treatment of cationic complex **1** with PhSH at room temperature results in a new set of ^{31}P NMR resonances at 74.6 ppm and 6.8 ppm corresponding to the central NHP phosphorus and an equivalent set of phosphine sidearms, respectively. The upfield shift in the central NHP resonance by comparison to starting material **1** (δ 198.8 ppm) suggests oxidative addition of the S–H bond across the Pt–P^{NHP} bond to generate [(PP(H)P)Pt(SPh)]-[PF_6] (**3**), as shown in Scheme 2. The formulation of complex **3** is confirmed by the absence of a ^1H NMR resonance indicative of a Pt-hydride and an upfield-shifted doublet at 7.63 ppm ($^1J_{P-H}$ = 438 Hz) corresponding to a phosphorus-bound proton. Likewise, the $^1J_{P-H}$ obtained from the proton-coupled ^{31}P NMR spectrum of **3** is identical.

In contrast, PhOH does not react with **1** at room temperature. Upon heating, however, a new product gradually forms over the course of several days. Similar to **3**, this new product has a dramatically upfield-shifted ^{31}P NMR resonance at 89.9 ppm for the central NHP phosphorus and a single resonance at −15.7 ppm corresponding to the phosphine sidearms. An additional ^{31}P NMR signal at 7.8 ppm is indicative of bound PPh_3. The most diagnostic spectroscopic feature and the most pronounced difference from **3**, however, is the clear presence of a Pt-hydride, indicated by a multiplet at −10.27 ppm in the ^1H NMR of the phenol addition product. Thus, the O–H bond also oxidatively adds across the Pt–P bond of **1**, but in a different manner resulting in formation of [(PP(OPh)P)Pt(H)(PPh_3)][PF_6] (**4**), as shown in Scheme 2. Alkyl-substituted alcohols such as methanol react similarly with **1** to generate similar products such as [(PP(OMe)-P)Pt(H)(PPh_3)][PF_6] (**5**).

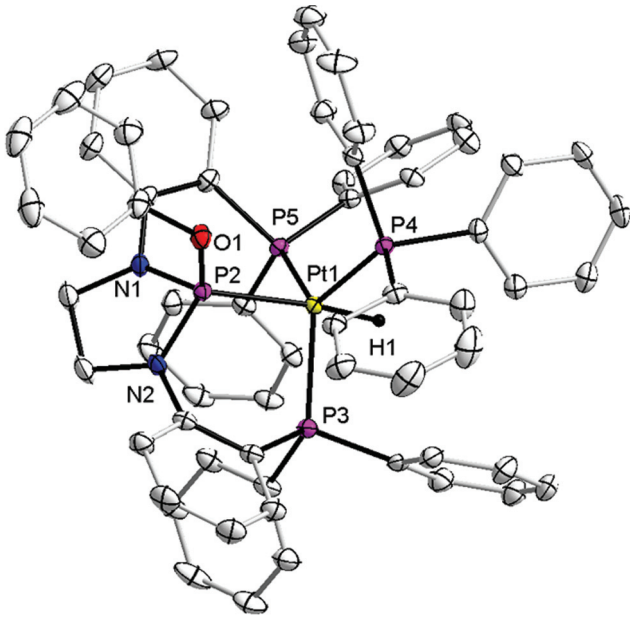

Fig. 1 Displacement ellipsoid representation (50%) of **4**. For clarity, hydrogen atoms, the PF_6^- counteranion, and solvate molecules have been omitted. Relevant bond distances (Å) and angles (°): Pt–P2, 2.2445 (9); Pt–P3, 2.3240(9); Pt–P4, 2.3573(9); Pt–P5, 2.3018(9); P2–O1, 1.625(3); P2–Pt1–P3, 90.29(3); P2–Pt–P4, 101.62(3); P3–Pt–P4, 111.77(3); P2–Pt–P5, 89.89(3); P3–Pt–P5, 126.32(3); P4–Pt–P5, 120.68(3); Pt–P2–O1, 112.38(11).

The solid-state structure of **4** was determined crystallographically and is shown in Fig. 1. The geometry about Pt is approximately trigonal bipyramidal (τ = 0.7),[38] with the NHP-derived heterocycle and the hydride occupying axial positions. The Pt–P^{NHP} distance of 2.2445(9) Å is similar to that in starting material **1** (2.2600(7) Å),[30] in stark contrast to literature examples.[39,40] For instance, in $(CO)_4Mo(NHP^{Me})(NHP^{Me}OMe)$ the Mo–P distance associated with the MeO-substituted NHP is ~0.2 Å longer than the Mo–P distance associated with the NHP unit.[39] This case differs from the comparison of **4** with **1**, however, in that the NHP in the Mo system adopts a planar geometry and is formally an NHP^+ phosphenium with a double bond to Mo, while the NHP in **4** is a pyramidal phosphite fragment with a single bond to Pt. Addition of a phenoxy group to the NHP fragment in **1** changes the nature of the M–P bond, but in this case it does not serve to disrupt multiple bonding.

Since 1,2-addition of S–H and O–H bonds led to different products, complex **1** was also treated with one equivalent of HCl to probe the preference for product formation as a function of acidity. The product of this reaction, [(PP(H)P)PtCl][PF_6] ($\mathbf{6^{PF6}}$),

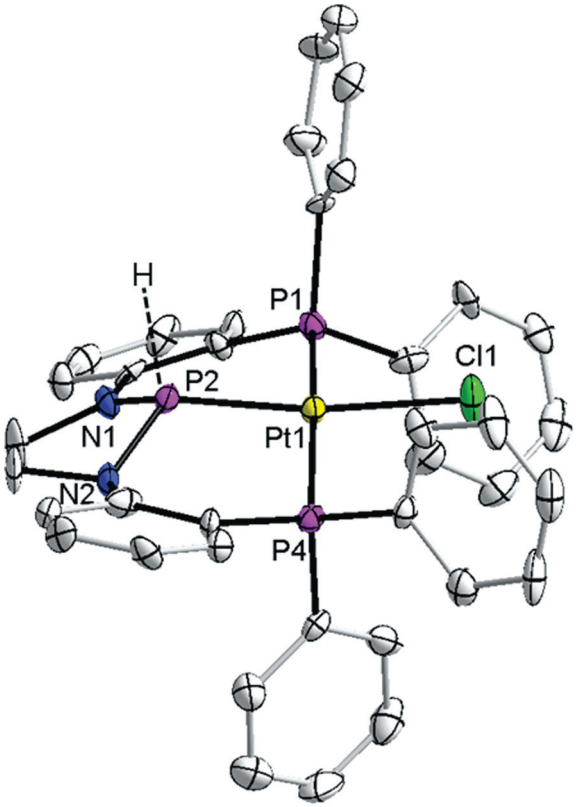

Fig. 2 Displacement ellipsoid representation (50%) of $\mathbf{6}^{\mathbf{PF6}}$. For clarity, hydrogen atoms and the PF_6^- counteranion have been omitted and only one of the two molecules in the asymmetric unit is shown. In addition only one of the two disordered position of the central NHP phosphorus is shown. Relevant bond distances (Å): (molecule 1): Pt1–P2/P3, 2.162(2)/2.18(3); Pt–P4, 2.298(2); Pt–P1, 2.2906(19); Pt–Cl1, 2.354(2); (molecule 2): Pt11–P102/103, 2.212(4)/2.142(5); Pt11–P101, 2.308(2); Pt11–P104, 2.300(2).

is similar to that of PhSH, with proton addition to the central NHP phosphorus atom and coordination of the chloride anion to Pt. The absence of coordinated PPh_3 in **3** and $\mathbf{6}^{\mathbf{PF6}}$ is likely attributed to the greater steric demand of the thiolate and chloride ligands compared to the hydride ligand in **4** and **5**.

The solid-state structure of $\mathbf{6}^{\mathbf{PF6}}$ was determined *via* X-ray crystallography and is shown in Fig. 2. In both independent molecules in the asymmetric unit, the central NHP phosphorus atom is disordered over two positions. This disorder was modelled adequately, but prevented the detection of the hydrogen atom bound to P. Its presence, however, is unequivocal based on ^{1}H NMR data and based on the balancing of charge in this diamagnetic molecule. The structure reveals a square planar geometry about Pt with a Pt–P^{NHP} distance significantly shorter than in **4** or in the starting material **1**. Rather than invoking an argument about the NHP–H's donor ability, this phenomenon can be explained by the poorer *trans* influence of Cl^- by comparison to PR_3 or H^-.

From the above results, it appears that more acidic E–H bonds (HCl, thiols) lead to the protonation of the central NHP phosphorus atom, while less acidic E–H bonds (phenol and alcohols) lead to the opposite selectivity. The phosphido character of the central NHP phosphorus atom suggests that initial protonation of

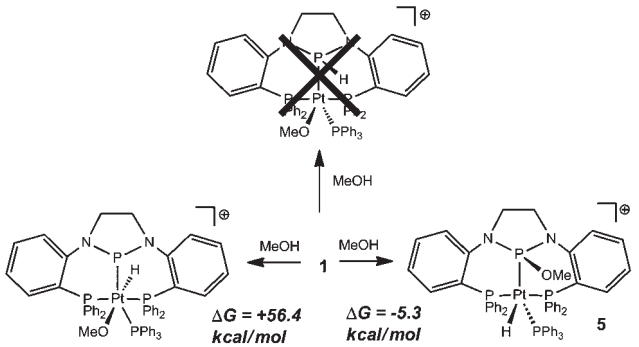

Scheme 3 Calculated energies of several possible products of MeOH addition to **1**.

the NHP phosphorus atom may be the key step in the preferential formation of **3** and $\mathbf{6}^{\mathbf{PF6}}$. However, the outcomes of these E–H addition reactions could also be a consequence of preferences dictated by hard–soft acid–base theory; *i.e.*, the oxophilic nature of phosphorus. Upon examination of literature examples of cleavage of E–H bonds across M=PR_2 bonds, one can observe that in cases of O–H bond heterolysis OR^- always ends up on P,[33–35] while two reported examples of S–H cleavage result in M–SR species.[36,37] Moreover, in a few control experiments with more acidic phenol derivatives (pentafluorophenol and 2,4,6-trichlorophenol) products similar to **4** were observed as the exclusive products by NMR spectroscopy. Thus, acidity does not seem to exclusively dictate the selectivity of 1,2-addition, and hard–soft preferences clearly play an important role.

A computational investigation on the selectivity of these reactions was carried out using density functional theory (DFT). Upon first examining the possible products of the reaction of **1** with MeOH, we find that **5** is the lowest energy product (ΔG = −5.3 kcal mol^{-1}). Attempts to optimize the geometry of the Pt-methoxide product $[(PP(H)P)Pt(OMe)(PPh_3)]^+$ were unsuccessful and resulted in *in silico* dissociation of PPh_3 to give $[(PP(H)P)Pt(OMe)]^+$. As shown in Scheme 3, the product of oxidative addition of MeOH directly to Pt without involvement from the NHP moiety is too high in energy (ΔG = 56.4 kcal mol^{-1}) to contribute to the reaction pathway. Since it is also possible that the PPh_3 dissociates prior to oxidative addition to generate an NHP^+ phosphenium intermediate, we also examined the reaction of the three-coordinate $[(PPP)Pt]^+$ species with PhOH (Scheme 4). In this case, not only is the (PP(OPh)P)PtH product lower in energy than the (PP(H)P)PtOPh product (ΔG = −6.4 and 14.8 kcal mol^{-1}, respectively), the computed activation energy for formation of the Pt-hydride product is also significantly lower ($\Delta G^{\ddagger}$ = 37.2 kcal mol^{-1} compared to 50.0 kcal mol^{-1}). In the case of PhSH, where the isolated product is a Pt-thiolate with apparent protonation of the central NHP unit, the computed energies differences cannot be interpreted in such a straightforward manner. As shown in Scheme 5, in the reaction of $[(PPP)Pt]^+$ with PhSH, the Pt-hydride species is predicted to be the thermodynamically favored product by *ca.* 8 kcal mol^{-1}. However, both products are shown to be energetically uphill from the three coordinate Pt starting material. Thus, in this case, we propose that it is important that PPh_3 remain coordinated (keeping the NHP unit in an NHP^- phosphido configuration) upon PhSH addition.

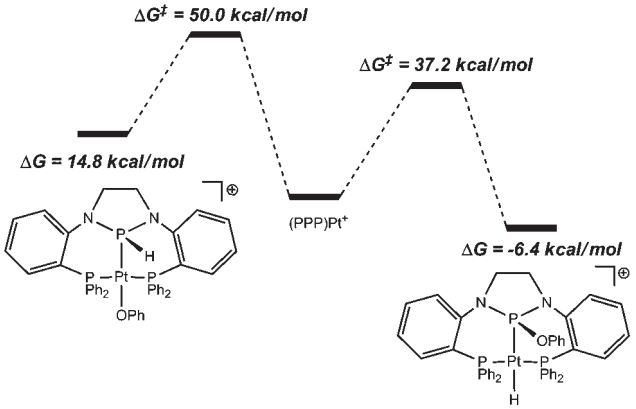

Scheme 4 Calculated reaction pathway of the addition of PhOH to $[(PPP)Pt]^+$.

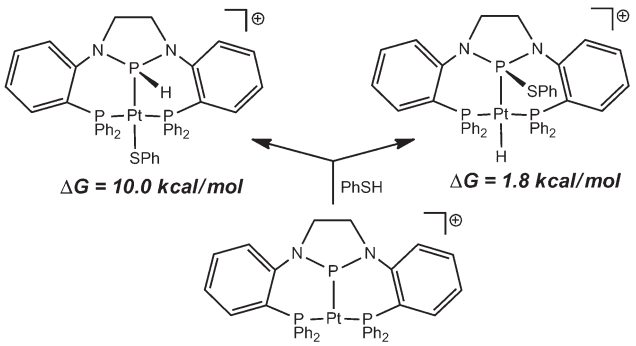

Scheme 5 Calculated energetics of the reaction of $[(PPP)Pt]^+$ with PhSH.

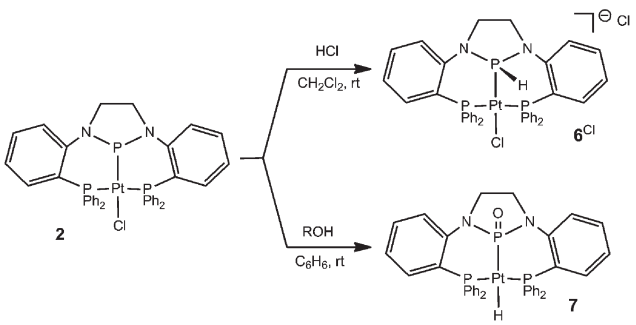

Scheme 6 Addition of E–H bonds to **2**.

Heterolytic cleavage of E–H bonds by (PPP)PtCl (2)

Element–hydrogen bond addition was also investigated starting with the neutral NHP complex **2**. Addition of HCl proceeded similarly, affording a similar product [(PP(H)P)PtCl][Cl] (**6^{Cl}**, Scheme 6). PhSH addition to **2** also afforded a product spectroscopically identical to **3**, although presumably with a Cl^- counteranion in place of PF_6^-.

In contrast, treatment of **2** with PhOH resulted in no reaction, even in refluxing benzene for extended periods of time. Presumably complex **2** is less reactive than **1** owing to the stronger coordination of Cl^- to Pt. Unlike the reaction with phenol, **2** reacts readily with MeOH but yields a product vastly different from **5**: While a Pt-hydride signal is still observed in the ^{1}H NMR of the product at −1.80 ppm and the ^{31}P resonance for the central phosphorus is shifted downfield to 86.7 ppm, no signal attributable to a methyl group could be identified. Moreover, EtOH addition to **2** resulted in a spectroscopically identical product. The product was, therefore, tentatively assigned as (PP(O)P)Pt(H) (**7**, Scheme 6). Notably, the RCl byproduct was observed *via* both GC-MS and ^{1}H NMR spectroscopy upon completion of the reaction.

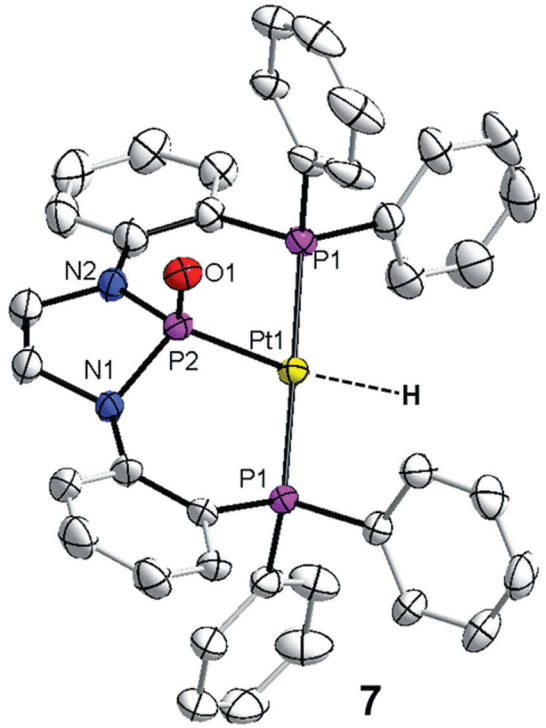

Fig. 3 Displacement ellipsoid representation (50%) of **7**. For clarity, hydrogen atoms have been omitted and only one of two disordered positions is shown. Relevant bond distances (Å) and angles (°): Pt–P1, 2.2586(7); Pt–P2, 2.2242(14); P2–O1, 1.485(4); P2–N2, 1.709(5); P2–N1, 1.725(5); P1–Pt–P1, 177.86(4); Pt–P2–O1, 119.64(18).

The solid-state structure of **7** confirms its formulation as an *N*-heterocyclic phosphinito Pt-hydride complex (Fig. 3). While the hydride could not be located in the difference Fourier map, its location can be geometrically inferred. The geometry around the Pt center is essentially square planar once the hydride's supposed position is taken into account. The Pt–P^{NHP} distance (2.2242(14) Å) is nearly identical to that in the unoxidized (PPP)PtBr complex,[30] and similar to the Pd–P distance in Bourissou's similar pincer complex $\{[o\text{-}^i Pr_2P(C_6H_4)]_2P(=O)Ph\}Pd(Ph)$.[41] This trend is in stark contrast to the previously observed ~0.07 Å contraction of the Co–P^{NHP} distance upon oxidation of the central phosphorus in $(PPP)Co(CO)_2$ to $(PP(O)P)Co(CO)_2$;[29] however, chloride-to-hydride substitution at the position *trans* to the central phosphorus atom likely contributes to the P^{NHP}–Pt bond distance in this case as well.

The mechanism by which the unusual product **7** is formed deserves consideration. There are a number of literature examples of transition metal phosphites undergoing dealkylation

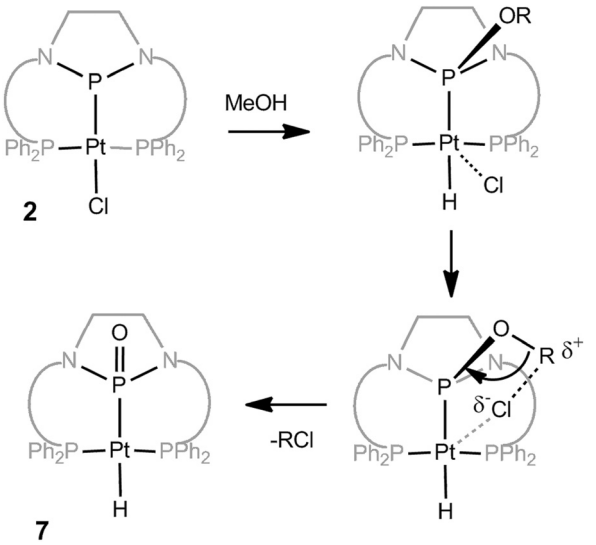

Scheme 7 Proposed mechanism for formation of **7** from **2** and MeOH.

reactions *via* an Arbuzov-type reaction,[42] although to our knowledge this type of reactivity is unprecedented in *N*-heterocyclic phosphite systems. Transition metal phosphite dealkylation usually proceeds *via* either an ionic or radical mechanism, with the former being more common in the presence of nucleophiles such as halides. Thus, we propose that a plausible pathway involves initial oxidative addition of MeOH to **2** to form an intermediate Pt-hydride species similar to **4**, followed by an intramolecular S_N2 reaction between the Pt-bound Cl^- and the methoxy carbon (Scheme 7). Notably, the Pt–Br and Pt–I analogues of **2** also lead to **7** upon ROH addition.

Conclusions

In summary, we have shown that the E–H bonds of alcohols, thiols, and hydrochloric acid add to Pt–NHP complexes *via* oxidative addition across the Pt–P^{NHP} bond. In all cases, the oxidation state of Pt remains the same. Based on hard–soft acid/base preferences, the products of 1,2-addition of O–H and S–H bonds vary: Pt–H/P–OR products form preferentially in the O–H bond cleavage case, while Pt–SR/P–H products form from S–H addition reactions. Addition of HCl to Pt–NHP complexes also exclusively form Pt–Cl/P–H products, but based on control reactions with more acidic phenols we have established that product preferences are not pH-controlled. Interestingly, in the presence of nucleophilic halides, the P–OR phosphite products generated *via* addition of alcohols undergo an Arbuzov-like dealkylation reaction to release RX and generate an oxidized P═O phosphinito product. The participation of the NHP moiety in reactions of this type are further proof of the non-innocent nature of these ligands.

Experimental

General considerations

All syntheses reported were carried out using standard glovebox and Schlenk techniques in the absence of water and dioxygen, unless otherwise noted. Benzene, n-pentane, tetrahydrofuran, toluene, diethyl ether, and dichloromethane were degassed and dried by sparging with ultra high purity argon gas followed by passage through a series of drying columns using a Seca Solvent System by Glass Contours. All solvents were stored over 3 Å molecular sieves. Deuterated solvents were purchased from Cambridge Isotope Laboratories, Inc., degassed *via* repeated freeze-pump-thaw cycles, and dried over 3 Å molecular sieves. Solvents were frequently tested using a standard solution of sodium benzophenone ketyl in tetrahydrofuran to confirm the absence of oxygen and moisture. Complexes **1** and **2** were synthesized using literature procedures.[30] Thiophenol, phenol, methanol, ethanol and 1.0 M HCl solution in diethyl ether were purchased from commercial vendors and used without further purification. NMR spectra were recorded at ambient temperature unless otherwise stated on Varian Inova 400 MHz instrument. ^1H and ^{13}C NMR chemical shifts were referenced to residual solvent and are reported in ppm. ^{31}P NMR chemical shifts (in ppm) were referenced to 85% H_3PO_4 (0 ppm). Elemental microanalyses were performed by Complete Analysis Laboratories, Inc., Parsippany, NJ.

Synthesis of [(PP(H)P)Pt(SPh)][PF_6] (3)

Complex **1** (74.5 mg, 0.0615 mmol) was dissolved in THF (10 mL). To this orange solution was added thiophenol (6.3 μL, 0.062 mol). The reaction mixture became a yellow solution in 15 minutes. Removal of the volatiles *in vacuo* afforded a yellow solid as crude product. Crystallization of the crude product *via* vapor diffusion of diethyl ether into a concentrated THF solution yielded analytically pure product as yellow crystals. Yield: 75.6 mg, 93.0%. ^1H NMR (400 MHz, CD_2Cl_2): δ 7.65 (t, 2H, Ar-*H*), 7.63 (dd, 1H, P-*H*, $^1J_{P-H}$ = 438 Hz, $^2J_{Pt-H}$ = 160 Hz), 7.55 (m, 2H, Ar-*H*), 7.49 (m, 9H, Ar-*H*), 7.32 (t, 4H, Ar-*H*), 7.27 (t, 4H, Ar-*H*), 7.22 (m, 2H, Ar-*H*), 7.09 (t, 2H, Ar-*H*), 6.97 (m, 2H, Ar-*H*), 6.71 (t, 2H, Ar-*H*), 6.66 (m, 2H, Ar-*H*), 6.57 (t, 2H, Ar-*H*), 3.91 (m, 2H, C*H*2), 3.77 (m, 2H, C*H*2). ^{31}P NMR (161.8 MHz, CD_2Cl_2): δ 74.6 (ddt, 1P, $^1J_{Pt-P}$ = 2716 Hz, $^1J_{P-H}$ = 438 Hz, $^2J_{P-P}$ = 36 Hz), 6.8 (dd, 2P, $^1J_{Pt-P}$ = 2295 Hz, $^2J_{P-P}$ = 36 Hz), −143.9 (sept, 1P, $^1J_{P-F}$ = 710 Hz). ^{13}C NMR (100.5 MHz, CD_2Cl_2): δ 145.9, 135.9, 134.8, 134.5, 134.2, 132.7, 132.4, 132.3, 129.4, 128.8, 127.6, 123.7, 123.0, 118.6, 48.3. Anal. Calcd for $C_{44}H_{38}N_2F_6P_4PtS$: C, 49.86; H, 3.61; N, 2.64. Found: C, 49.81; H, 3.73; N, 2.69%.

Synthesis of [(PP(OPh)P)Pt(H)(PPh_3)][PF_6] (4)

Complex **1** (47.5 mg, 0.0392 mmol) was dissolved in dichloromethane (10 mL) and to this orange solution was added phenol (3.7 mg, 0.039 mmol). The mixture was heated in a sealed vessel in an oil bath at 60 °C for two days to ensure complete reaction. After completion, removal of the volatiles from the colorless solution *in vacuo* afforded white solid as analytically pure product. Yield: 48.7 mg, 95.1%. Colorless crystals suitable for X-ray crystallography were grown *via* vapor diffusion of n-pentane into a concentrated dichloromethane solution of **4**. ^1H NMR (400 MHz, CD_2Cl_2): δ 7.67 (t, 2H, Ar-*H*), 7.31 (m, 6H, Ar-*H*), 7.26–7.19 (m, 8H, Ar-*H*), 7.18–7.03 (m, 30H, Ar-*H*),

6.23 (d, 2H, Ar-*H*), 3.43 (m, 2H, C*H*2), 3.14 (m, 2H, C*H*2), −10.27 (dd, 1H, Pt-*H*, $^{1}J_{Pt-H}$ = 670 Hz, $^{2}J_{P-H}$ = 280 Hz). ^{31}P NMR (161.8 MHz, CD_2Cl_2): δ 89.9 (dd, 1P, $^{1}J_{Pt-P}$ = 2576 Hz, $^{2}J_{P-H}$ = 280 Hz), 7.8 (br, 1P, *P*Ph$_3$), −15.7 (d, 2P, $^{1}J_{Pt-P}$ = 2747 Hz), −143.9 (sept, 1P, $^{1}J_{P-F}$ = 710 Hz). ^{13}C NMR (100.5 MHz, CD_2Cl_2): δ 146.1, 135.4, 134.3, 133.8, 133.7, 133.6, 133.2, 133.1, 131.8, 131.4, 130.1, 129.1, 128.6, 128.5, 126.2, 124.3, 122.3, 121.3, 48.1. Anal. Calcd for $C_{62}H_{53}N_2F_6OP_5Pt$: C, 57.02; H, 4.09; N, 2.14. Found: C, 56.91; H, 4.06; N, 2.23%.

Synthesis of [(PP(OMe)P)Pt(H)(PPh$_3$)][PF$_6$] (5)

Complex **1** (44.3 mg, 0.0366 mmol) was dissolved in dichloromethane (10 mL) and to this orange solution was added MeOH (1.6 μL, 0.040 mmol). The mixture was allowed to stir at rt for 12 hours to ensure complete reaction. Upon completion, removal of volatiles from the resulting colorless solution afforded white solid as analytically pure **5**. Yield: 39.5 mg, 86.9%. ^{1}H NMR (400 MHz, CD_2Cl_2): δ 7.63 (t, 2H, Ar-*H*), 7.42 (m, 2H, Ar-*H*), 7.31 (m, 8H, Ar-*H*), 7.17 (t, 2H, Ar-*H*), 7.08 (m, 27H, Ar-*H*), 6.98 (m, 2H, Ar-*H*), 4.48 (m, 2H, C*H*2), 3.32 (m, 2H, C*H*2), 3.02 (d, 3H, OCH_3, $^{2}J_{P-H}$ = 12 Hz), −10.32 (dd, 1H, Pt-*H*, $^{1}J_{Pt-H}$ = 664 Hz, $^{2}J_{P-H}$ = 275 Hz). ^{31}P NMR (161.8 MHz, CD_2Cl_2): δ 94.6 (dd, 1P, $^{1}J_{Pt-P}$ = 2530 Hz, $^{2}J_{P-H}$ = 275 Hz), 9.8 (br, 1P, *P*Ph$_3$), −14.4 (d, 2P, $^{1}J_{Pt-P}$ = 2830 Hz), −143.9 (sept, 1P, $^{1}J_{P-F}$ = 710 Hz). ^{13}C NMR (100.5 MHz, CD_2Cl_2): δ 145.3, 134.9, 133.7, 133.6, 133.0, 132.7, 131.0, 130.3, 130.1, 128.8, 128.5, 128.4, 125.2, 124.5, 54.1, 49.3. Anal. Calcd for $C_{57}H_{51}N_2F_6OP_5Pt$: C, 55.03; H, 4.13; N, 2.25. Found: C, 55.08; H, 4.25; N, 2.21%.

Synthesis of [(PP(H)P)PtCl][PF$_6$] (6^{PF6})

Complex **1** (60.6 mg, 0.0500 mmol) was dissolved in dichloromethane (10 mL) and to this orange solution was added HCl (55 μL, 1.0 M HCl in diethyl ether, 0.0550 mmol). The mixture became colorless within ten seconds of addition. Removal of the volatiles from the colorless solution *in vacuo* afforded light yellow solid as analytically pure product **6^{PF6}**. Yield: 38.1 mg, 77.3%. Light yellow crystals suitable for X-ray crystallography were grown *via* vapor diffusion of n-pentane into a concentrated dichloromethane solution of complex **6^{PF6}**. ^{1}H NMR (400 MHz, CD_2Cl_2): δ 7.70 (t, 2H, Ar-*H*), 7.62 (m, 2H, Ar-*H*), 7.58 (m, 6H, Ar-*H*), 7.57 (dd, 1H, P-*H*, $^{1}J_{P-H}$ = 465 Hz, $^{2}J_{Pt-H}$ = 235 Hz), 7.49 (m, 8H, Ar-*H*), 7.42 (m, 4H, Ar-*H*), 7.31 (m, 2H, Ar-*H*), 7.12 (t, 2H, Ar-*H*), 6.98 (m, 2H, Ar-*H*), 4.10 (m, 2H, C*H*2), 3.83 (m, 2H, C*H*2). ^{31}P NMR (161.8 MHz, CD_2Cl_2): δ 64.1 (ddt, 1P, $^{1}J_{Pt-P}$ = 3596 Hz, $^{1}J_{P-H}$ = 465 Hz, $^{2}J_{P-P}$ = 29 Hz), 6.4 (dd, 2P, $^{1}J_{Pt-P}$ = 2200 Hz, $^{2}J_{P-P}$ = 29 Hz), −143.9 (sept, 1P, $^{1}J_{P-F}$ = 710 Hz). ^{13}C NMR (100.5 MHz, CD_2Cl_2): δ 145.8, 134.9, 134.7, 134.5, 132.9, 132.6, 129.7, 129.2, 123.5, 119.1, 47.8. Anal. Calcd for $C_{38}H_{33}N_2ClF_6P_4Pt$: C, 46.28; H, 3.37; N, 2.84. Found: C, 46.22; H, 3.42; N, 2.76%.

Synthesis of [(PP(H)P)PtCl][Cl] (6^{Cl})

Complex **2** (69.0 mg, 0.0821 mmol) was dissolved in dichloromethane (10 mL). To this yellow solution was added HCl (90 μL, 1.0 M solution in diethyl ether, 0.090 mmol). The reaction mixture became a lighter yellow color within ten seconds of addition. Removal of the volatiles from the colorless solution *in vacuo* afforded yellow solid as analytically pure product. Yield: 70.0 mg, 97.2%. ^{1}H NMR (400 MHz, CD_2Cl_2): δ 7.87 (dd, 1H, P-*H*, $^{1}J_{P-H}$ = 472 Hz, $^{2}J_{Pt-H}$ = 239 Hz), 7.69 (t, 2H, Ar-*H*), 7.60 (m, 2H, Ar-*H*), 7.54–7.40 (m, 20H, Ar-*H*), 7.09 (t, 2H, Ar-*H*), 6.97 (m, 2H, Ar-*H*), 4.38 (m, 2H, C*H*2), 3.85 (m, 2H, C*H*2). ^{31}P NMR (161.8 MHz, CD_2Cl_2): δ 64.1 (ddt, 1P, $^{1}J_{Pt-P}$ = 3560 Hz, $^{1}J_{P-H}$ = 472 Hz, $^{2}J_{P-P}$ = 29 Hz), 6.9 (dd, 2P, $^{1}J_{Pt-P}$ = 2194 Hz, $^{2}J_{P-P}$ = 29 Hz), −143.9 (sept, 1P, $^{1}J_{P-F}$ = 710 Hz). ^{13}C NMR (100.5 MHz, CD_2Cl_2): δ 146.1, 134.9, 134.8, 134.4, 132.8, 132.4, 129.6, 129.2, 123.2, 119.7, 48.3. Anal. Calcd for $C_{38}H_{33}N_2Cl_2P_3Pt$: C, 52.07; H, 3.79; N, 3.20. Found: C, 52.81; H, 3.98; N, 2.96%.

Synthesis of (PP(O)P)Pt(H) (7)

Complex **2** (22 mg, 0.026 mmol) was stirred in benzene (10 mL) and to this yellow suspension was added MeOH (1.2 μL, 0.030 mmol). The mixture was allowed to stir at rt for 12 hours to ensure complete reaction. Upon completion, removal of volatiles from the resulting yellow solution afforded yellow solid as crude product. Yield: 18.5 mg, 86.0%. Purification of the crude product *via* vapor diffusion of n-pentane into a concentrated dichloromethane solution of the crude product afforded yellow crystals suitable for X-ray crystallography. ^{1}H NMR (400 MHz, CD_2Cl_2): δ 7.71 (m, 2H, Ar-*H*), 7.63 (m, 2H, Ar-*H*), 7.49–7.36 (m, 18H, Ar-*H*), 7.04–6.96 (m, 4H, Ar-*H*), 6.82 (m, 2H, Ar-*H*), 4.17 (m, 2H, C*H*2), 3.46 (m, 2H, C*H*2), −1.80 (ddt, 1H, $^{1}J_{Pt-H}$ = 950 Hz, $^{2}J_{NHP-H}$ = 184 Hz, $^{2}J_{P(Ar)-H}$ = 16 Hz). ^{31}P NMR (161.8 MHz, CD_2Cl_2): δ 86.7 (ddt, 1P, $^{1}J_{Pt-P}$ = 2260 Hz, $^{1}J_{P-H}$ = 184 Hz, $^{2}J_{P-P}$ = 43 Hz), 5.1 (dd, 2P, $^{1}J_{Pt-P}$ = 2607 Hz, $^{2}J_{P-P}$ = 43 Hz). ^{13}C NMR (100.5 MHz, CD_2Cl_2): δ 150.7, 136.3, 134.4, 134.0, 133.0, 131.0, 130.7, 128.6, 119.4, 118.0, 45.9. Anal. Calcd for $C_{38}H_{33}N_2OP_3Pt$: C, 55.55; H, 4.05; N, 3.41. Found: C, 55.49; H, 4.07; N, 3.33%.

X-ray crystallography procedures

All operations were performed on a Bruker-Nonius Kappa Apex2 diffractometer, using graphite-monochromated MoKα radiation. All diffractometer manipulations, including data collection, integration, scaling, and absorption corrections were carried out using the Bruker Apex2 software.[43] Preliminary cell constants were obtained from three sets of 12 frames. Crystallographic parameters are summarized in Table 1, and further experimental crystallographic details are described for each compound in the ESI.† Data in CIF format are also provided in a separate file.†

Computational methods

All calculations were performed using Gaussian09[44] for the Linux operating system. Density functional theory calculations were carried out using the B3LYP hybrid functional; Becke's three parameter exchange functional (B3)[45] and the correlation functional of Lee, Yang, and Parr (LYP).[46] A mixed-basis set

Table 1 Crystallographic data and refinement parameters for **4**, $\mathbf{6}^{\mathbf{PF6}}$, and **7**

	4·2CH_2Cl_2	$\mathbf{6}^{\mathbf{PF6}}$	**7**
Chemical formula	$C_{64}H_{57}Cl_4F_6N_2O_1P_5Pt_1$	$C_{38}H_{32}Cl_1F_6NP_4Pt_1$	$C_{38}H_{32}N_2O_1P_3Pt_1$
F_w	1475.93	985.11	820.70
T (K)	120	120	120
λ (Å)	0.71073	0.71073	0.71073
a (Å)	14.8742(10)	12.1189(4)	25.0443(7)
b (Å)	35.625(3)	13.4744(5)	15.9342(5)
c (Å)	11.9635(9)	22.8621(9)	9.6935(3)
β (°)	107.599(4)	98.743(2)	110.393(1)
V (Å^3)	6042.7(8)	3689.9(2)	3625.85(19)
Space group	$P2_1/c$	$P2_1$	$C2/c$
Z, Z'	4, 1	4, 2	4, 0.5
D_{calc} (g cm^{-3})	1.622	1.773	1.503
μ (cm^{-1})	26.95	41.1	40.33
R_{int}	0.048	0.044	0.032
N_{ref} (all), N_{ref} ($I > 2\sigma(I)$)	17 579, 14 355	21 159, 17 543	5303, 4020
R_1 ($I > 2\sigma(I)$), wR_2 [a] (all)	0.0418, 0.1067	0.0419, 0.0835	0.0242, 0.0605

[a] $R_1 = \sum||F_o| - |F_o||/\sum|F_o|$; $wR_2 = \{\sum[w(F_o^2 - F_c^2)_2]/\sum[w(F_o^2)^2]\}^{1/2}$.

was employed, using the LANL2DZ(p,d) double zeta basis set with effective core potentials for phosphorus, iodine, and platinum[47–49] and Gaussian09's internal LANL2DZ basis set (equivalent to D95V[50]) for carbon, nitrogen, and hydrogen. Using crystallographically determined geometries as a starting point, the geometries were optimized to a minimum, followed by analytical frequency calculations to confirm that no imaginary frequencies were present. XYZ coordinates of the optimized geometries of all calculated complexes are provided in the ESI.†

Acknowledgements

The authors are thankful to Brandeis University for funding this project. C. Thomas is also grateful for a 2011 Alfred P. Sloan Fellowship.

Notes and references

1 G. Erker, *Dalton Trans.*, 2011, **40**, 7475–7483.
2 D. W. Stephan, S. Greenberg, T. W. Graham, P. Chase, J. J. Hastie, S. J. Geier, J. M. Farrell, C. C. Brown, Z. M. Heiden, G. C. Welch and M. Ullrich, *Inorg. Chem.*, 2011, **50**, 12338–12348.
3 D. W. Stephan and G. Erker, *Angew. Chem., Int. Ed.*, 2010, **49**, 46–76.
4 D. W. Stephan, *Dalton Trans.*, 2009, 3129–3136.
5 M. Sircoglou, S. Bontemps, M. Mercy, N. Saffon, M. Takahashi, G. Bouhadir, L. Maron and D. Bourissou, *Angew. Chem., Int. Ed.*, 2007, **46**, 8583–8586.
6 M. Sircoglou, S. b. Bontemps, G. Bouhadir, N. Saffon, K. Miqueu, W. Gu, M. Mercy, C.-H. Chen, B. M. Foxman, L. Maron, O. V. Ozerov and D. Bourissou, *J. Am. Chem. Soc.*, 2008, **130**, 16729–16738.
7 S. Bontemps, M. Sircoglou, G. Bouhadir, H. Puschmann, J. A. K. Howard, P. W. Dyer, K. Miqueu and D. Bourissou, *Chem.–Eur. J.*, 2008, **14**, 731–740.
8 M.-E. Moret and J. C. Peters, *Angew. Chem., Int. Ed.*, 2011, **50**, 2063–2067.
9 J. S. Figueroa, J. G. Melnick and G. Parkin, *Inorg. Chem.*, 2006, **45**, 7056–7058.
10 V. K. Landry, J. G. Melnick, D. Buccella, K. Pang, J. C. Ulichny and G. Parkin, *Inorg. Chem.*, 2006, **45**, 2588–2597.
11 K. Pang, S. M. Quan and G. Parkin, *Chem. Commun.*, 2006, 5015–5017.
12 G. Parkin, *Organometallics*, 2006, **25**, 4744–4747.
13 W. H. Harman and J. C. Peters, *J. Am. Chem. Soc.*, 2012, **134**, 5080–5082.
14 A. Amgoune and D. Bourissou, *Chem. Commun.*, 2011, **47**, 859–871.
15 T.-P. Lin, C. R. Wade, L. M. Pérez and F. P. Gabbaï, *Angew. Chem., Int. Ed.*, 2010, **49**, 6357–6360.
16 C. R. Wade, T.-P. Lin, R. C. Nelson, E. A. Mader, J. T. Miller and F. P. Gabbai, *J. Am. Chem. Soc.*, 2011, **133**, 8948–8955.
17 C. R. Wade and F. P. Gabbaï, *Angew. Chem., Int. Ed.*, 2011, **50**, 7369–7372.
18 T.-P. Lin, R. C. Nelson, T. Wu, J. T. Miller and F. P. Gabbai, *Chem. Sci.*, 2012, **3**, 1128–1136.
19 C. R. Wade, I.-S. Ke and F. P. Gabbaï, *Angew. Chem., Int. Ed.*, 2012, **51**, 478–481.
20 C. M. Thomas, *Comments Inorg. Chem.*, 2011, **32**, 14–38.
21 R. K. Bansal and D. Gudat, *Phosphorus Heterocycles II*, Springer, Berlin/Heidelberg, vol. 21, pp. 63–102.
22 D. Gudat, *Coord. Chem. Rev.*, 1997, **163**, 71–106.
23 D. Gudat, *Acc. Chem. Res.*, 2010, **43**, 1307–1316.
24 K. Takano, H. Tsumura, H. Nakazawa, M. Kurakata and T. Hirano, *Organometallics*, 2000, **19**, 3323–3331.
25 D. Gudat, *Eur. J. Inorg. Chem.*, 1998, 1087–1094.
26 D. Gudat, A. Haghverdi, H. Hupfer and M. Nieger, *Chem.–Eur. J.*, 2000, **6**, 3414–3425.
27 B. Pan and C. M. Thomas, Unpublished results.
28 G. S. Day, B. Pan, D. L. Kellenberger, B. M. Foxman and C. M. Thomas, *Chem. Commun.*, 2011, **47**, 3634–3636.
29 B. Pan, M. W. Bezpalko, B. M. Foxman and C. M. Thomas, *Organometallics*, 2011, **30**, 5560–5563.
30 B. Pan, Z. Xu, M. W. Bezpalko, B. M. Foxman and C. M. Thomas, *Inorg. Chem.*, 2012, **51**, 4170–4179.
31 L. C. Gregor, C.-H. Chen, C. M. Fafard, L. Fan, C. Guo, B. M. Foxman, D. G. Gusev and O. V. Ozerov, *Dalton Trans.*, 2010, **39**, 3195–3202.
32 M. A. Dureen, G. C. Welch, T. M. Gilbert and D. W. Stephan, *Inorg. Chem.*, 2009, **48**, 9910–9917.
33 M. A. Esteruelas, A. M. López, J. I. Tolosa and N. Vela, *Organometallics*, 2000, **19**, 4650–4652.
34 K. Jörg, W. Malisch, W. Reich, A. Meyer and U. Schubert, *Angew. Chem.*, 1986, **98**, 103–104.
35 R. Wein and H. Werner, *Chem. Ber.*, 1986, **119**, 2055–2058.
36 D. M. Stefanescu, H. F. Yuen, D. S. Glueck, J. A. Golen, L. N. Zakharov, C. D. Incarvito and A. L. Rheingold, *Inorg. Chem.*, 2003, **42**, 8891–8901.
37 M. M. Hossain, H.-M. Lin and S.-G. Shyu, *Organometallics*, 2003, **22**, 3262–3270.
38 A. W. Addison, T. N. Rao, J. Reedijk, J. van Rijn and G. C. Verschoor, *J. Chem. Soc., Dalton Trans.*, 1984, 1349–1356.
39 H. Nakazawa, Y. Miyoshi, T. Katayama, T. Mizuta, K. Miyoshi, N. Tsuchida, A. Ono and K. Takano, *Organometallics*, 2006, **25**, 5913–5921.
40 H. Nakazawa, Y. Yamaguchi, T. Mizuta and K. Miyoshi, *Organometallics*, 1995, **14**, 4173–4182.

41 E. J. Derrah, S. Ladeira, G. Bouhadir, K. Miqueu and D. Bourissou, *Chem. Commun.*, 2011, **47**, 8611–8613.
42 T. B. Brill and S. J. Landon, *Chem. Rev.*, 1984, **84**, 577–585.
43 Bruker Analytical X-ray Systems, Madison, WI, 2006.
44 M. J. Frisch, G. W. Trucks, H. B. Schlegel, G. E. Scuseria, M. A. Robb, J. R. Cheeseman, G. Scalmani, V. Braone, B. Mennucci and G. A. Petersson, *et al.*, Gaussian, Inc., Wallingford, CT, 2009.
45 A. D. Becke, *J. Chem. Phys.*, 1993, **98**, 5648–5652.
46 C. Lee, W. Yang and R. G. Parr, *Phys. Rev. B*, 1988, **37**, 785–789.
47 P. J. Hay and W. R. Wadt, *J. Chem. Phys.*, 1985, **82**, 270–283.
48 P. J. Hay and W. R. Wadt, *J. Chem. Phys.*, 1985, **82**, 299–310.
49 P. J. Hay and W. R. Wadt, *J. Chem. Phys.*, 1985, **82**, 284–298.
50 T. H. Dunning and P. J. Hay, in *Modern Theoretical Chemistry*, ed. H. F. Schaefer, Plenum, New York, 1976, vol. 3, pp. 1–28.